Effect of Grain Shape and Relative Humidity on the Nonlinear Elastic Properties of Granular Media

L. Gao[1], P. Shokouhi[1], and J. Rivière[1]

[1] Department of Engineering Science and Mechanics, Pennsylvania State University, University Park, Pennsylvania 16802, USA.

Corresponding author: Linying Gao(lzg245@psu.edu)

Key Points:

- The elastic nonlinearity of spherical particles increases with relative humidity increase, while it is rather constant in angular particles.
- We attribute this RH independence in sand to grain interlocking that prevents adsorbed water from weakening the grain junctions.
- For angular particles, we observe an amplitude threshold above which grain junctions start to unlock and where sliding/partial slip occurs.

Abstract

This study focuses on unraveling the microphysical origins of the nonlinear elastic effects, which are pervasive in the Earth's crust. Here, we examine the influence of grain shape and relative humidity (RH) on the elastic nonlinearity of granular assemblies made of spherical glass beads and angular sand particles. We find that their elastic nonlinearity is of the same order of magnitude. However, while the elastic nonlinearity of glass beads increases with RH, that of sand particles is rather RH independent. We attribute this difference to the angularity of sand particles; absorbed water on the spherical grains weakens the junctions making them more nonlinear, while no such effect occurs in sand due to grain interlocking. Additionally, for one of the nonlinear parameters that likely arises from shearing/partial slip of the grain junctions, we observe a sharp amplitude threshold in sand which is not observed in glass beads.

1 Introduction

Nonlinear elastic effects arise in solids due to the presence of imperfections at the micro/mesoscopic scale, such as cracks or dislocations (Ostrovsky & Johnson, 2001). Understanding the origins of these nonlinear elastic effects is critical to numerous fields, from geophysics (Abeele et al., 2002; Delorey et al., 2021; Feng et al., 2018, 2022; Guyer & Johnson, 2009; Hillers et al., 2015; P. Johnson & Sutin, 2005; Manogharan et al., 2021; McCall & Guyer, 1994; Shokouhi et al., 2020; Tadavani et al., 2020; TenCate et al., 1996, 1996, 2016) and civil engineering (Abeele & De Visscher, 2000; Astorga et al., 2018; Bittner & Popovics, 2022; G. Kim et al., 2017; Lacouture et al., 2003; Payan et al., 2014; Shokouhi et al., 2017) to the non-destructive evaluation of materials (Breazeale & Ford, 1965; Buck et al., 1978; Jin et al., 2020; J.-Y. Kim et al., 2006; Matlack et al., 2015; Williams et al., 2022). Elastic nonlinearity is particularly large in poorly consolidated or unconsolidated materials, where it arises from weak junctions between grains (Brunet et al., 2008; Guyer & Johnson, 1999, 2009; Jia et al., 2011; P. A. Johnson & Jia, 2005; Langlois & Jia, 2014; Renaud et al., 2012; Rivière et al., 2015).

Previous work suggests that the nonlinear elastic response of consolidated granular media like rocks arises from two distinct mechanisms, one that might be related to the opening/closing of grain contacts, and the other one related to the shearing of grain junctions (Renaud et al., 2012; Rivière et al., 2015). To confirm this hypothesis and better understand the underlying physics, we seek to investigate the nonlinear elastic response of materials simpler than rocks, both in terms of composition and microstructural features. In our previous work (Gao et al., 2022), we studied the influence of relative humidity (RH) on the nonlinear elastic properties of glass bead samples. We found that all extracted nonlinear parameters increase with RH. If indeed both mechanisms exist, this suggests that they are affected similarly in glass beads and cannot be distinguished using changes in RH. In this study, we further attempt to distinguish both mechanisms, by investigating the role of grain shape on the nonlinear elastic properties of granular media. To do so, we use a technique called Dynamic Acousto-Elastic Testing (DAET), a pump-probe approach that allows one to retrieve the full nonlinear elastodynamic response of materials including hysteresis and transient weakening (Renaud et al., 2009, 2011). We carry out DAET measurements on samples of spherical glass beads and angular sand at various RH conditions, and hypothesize that shearing of grain junctions in samples composed of angular grains is more hindered than in samples made of spherical grains.

2 Materials and Methods

We prepare samples of spherical soda-lime glass beads (diameter 100-140μm, Mo-Sci Corporation, Rolla, Missouri) and angular, fine quartz sand (diameter 50-150μm, 99.8% SiO_2 with minor amounts of Fe_2O_3, Al_2O_3, <0.1% each, U.S. Silica Company) using a setup identical to our previous study (Gao et al., 2022). We place a 4.5 mm thick pack of granular media (i.e., glass beads or sand) on top of a steel block of area 10*10 cm^2. The sample is left overnight in a sealed bag with either desiccant or a 100% RH humid environment, for dry (~10% RH) and humid (100% RH) samples, respectively. The sample is then quickly taken out of the sealed bag and a second steel block of identical size is placed on top of the granular layer. The sides are sealed using multiple layers of tape. Two P-wave sensors with a central frequency of 1 MHz

(2.54 cm in diameter, V102-RM from Olympus, Waltham, MA) are placed at the bottom of blind holes inside the steel blocks – with a thin layer of molasses to ensure proper ultrasonic coupling – to track changes in elastic state. The sample assembly is then placed inside a loading apparatus. An on-board direct current displacement transducer (DCDT) is attached to the top steel block and referenced to the base of the loading apparatus to track thickness changes. A load cell is also placed in series between the sample and the hydraulic ram to measure force/stress. In addition to the eight experiments conducted with glass beads (reported in Gao et al., 2022), a total of fourteen experiments are conducted in sand, that is 22 experiments total.

A static stress of 4MPa is first applied to the sample with a hydraulic ram and maintained constant throughout the experiment via servocontrol. Dynamic oscillations are then superimposed to the static stress, also via servocontrol. We first apply two oscillation sets with 0.3 MPa peak amplitude for initial compaction and homogenization. Then we conduct four identical DAET oscillation sets with linearly increasing peak amplitudes ranging from 0.01 MPa to 0.3 MPa. Each oscillation set includes 15 oscillations, and each oscillation consists of 50 sinusoidal cycles at 10 Hz, separated by 20-second hold intervals. Detailed plots of stress and thickness versus time are shown in Fig. S1.

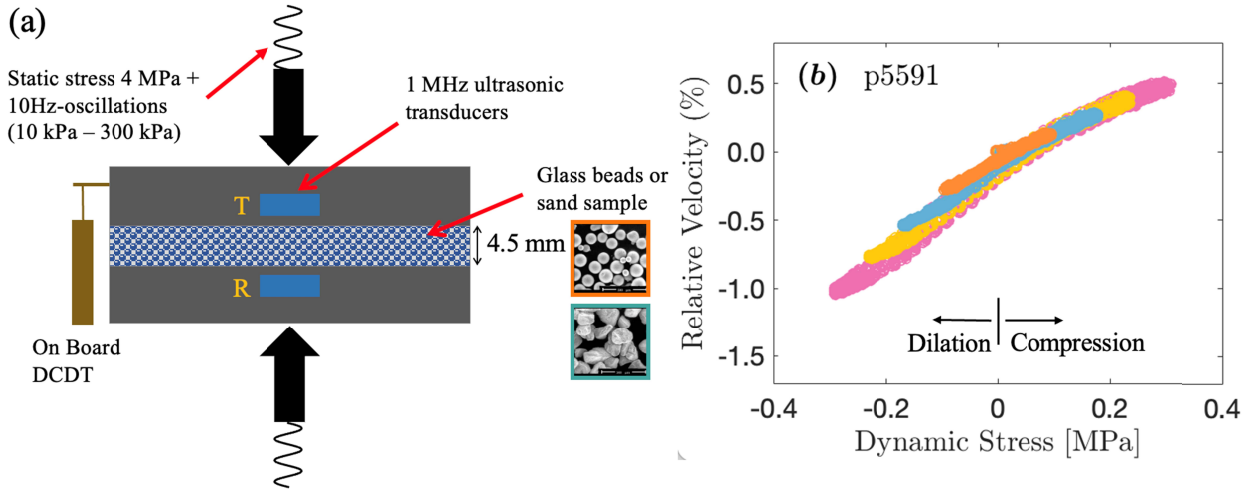

Figure 1. Experimental setup and typical result. (a) Experimental setup showing the loading apparatus and sample assembly. (b) Typical nonlinear signature (experiment p5591 is for a sand sample at 100% RH). Only 4 out of 15 dynamic stress levels are shown for clarity. The signatures for all 22 samples are shown in Figs. S4-5.

3 Data Analysis

After applying static stress to the sample, we measure the initial layer thickness with a caliper. We hand-pick the first arrival of a reference waveform (average of 50 consecutive waveforms taken after applying static stress) to estimate the initial time-of-flight. We then use thickness changes Δh measured with the displacement sensor and time-of-flight changes Δt estimated using

cross-correlation to calculate the wave velocity c throughout the experiment (Gao et al., 2022). Next, we compute the relative wave velocity change $\Delta c/c$ for each oscillation using $\Delta c/c = (c_{osc} - c_0)/c_0$, where c_0 represents the pre-oscillation wave velocity, and c_{osc} represents the wave velocity during the oscillation (Fig. S2). We can then generate the so-called nonlinear signatures by plotting relative velocity change $\Delta c/c$ as a function of dynamic stress (Fig. 1b).

To help us quantify the amount and type of elastic nonlinearity, we project the $\Delta c/c$ vs time signals onto a basis of sine and cosine functions at multiples (0, 1, 2) of the oscillation frequency (10 Hz). We then extract the magnitude of the harmonics R_n where $n = 0, 1, 2$. Using n up to 2 is shown to be sufficient to capture the complexity of the nonlinear signatures (Gao et al., 2022). The parameter R_0 characterizes the transient, average weakening occurring during the dynamic disturbance, while parameters R_1 and R_2 correspond approximately to the slope and curvature of the nonlinear signatures, respectively (Fig. S3). After obtaining the coefficients R_n, the dynamic stress dependence can be considered using the general formulation:

$$R_n = a_n \sigma^{\nu_n} \quad (1)$$

where, for a fixed n, a particular ν-value represents a particular type of nonlinearity (and associated physical mechanism), and the variable a represents how much of this mechanism or nonlinearity type is present in the sample. Taking logarithm (base 10) on both sides, Eq. 1 can be written as:

$$\log(R_n) = \nu_n \log(\sigma) + \log(a_n) \quad (2)$$

Plotting $\log(R_n)$ vs. $\log(\sigma)$, the slope ν_n tells us about the nonlinearity type, and the y-intercept ($\log(a_n)$) indicates how much nonlinearity is present.

4 Results and Discussion

Typical nonlinear signatures at four dynamic stress amplitudes are shown in Fig. 1b. Similar plots for the 22 samples are shown in Figs. S4-5. They all exhibit a similar positive correlation between wave velocity and dynamic stress, where as expected, the wave velocity is larger when dynamic stress is positive (compression phase), and smaller when dynamic stress is negative (dilation phase). We also observe that the slopes of the signature (R_1 component) dominate compared to the offset (R_0 component) and curvature (R_2 component), which is typical when pump and probe are aligned (vertical direction here, see Fig. 1a) (Renaud et al., 2013). Some rather large hysteresis can be observed for some of the samples, irrespective of RH level or grain shape. The reason behind the variability in hysteresis size is not clear and additional work would be required. Finally, we observe that for some samples, the slope appears larger during the dilation phase than during compression, suggesting that during the compression phase, the grain junctions are more tightly closed, producing smaller velocity changes (Figs. S4-5).

To obtain a quantitative assessment of the effect of grain shape and RH, we extract the harmonic content of all signatures. We calculate the Fourier series coefficients from the $\Delta c/c$ vs time signals at frequencies nf where f is the pump frequency (10 Hz) and $n = 0, 1, 2$. These coefficients, called R_n and representing the harmonic content, are shown in Fig. 2. The

harmonics are shown as a function of peak dynamic stress amplitude for both glass bead and sand samples, and under dry (~10%), humid (100%) as well as room humidity (~60%) conditions. On these log-log plots, following Eq. 2, the slope ν_n informs us about the nonlinearity type and the y-intercept ($\log(a_n)$) indicates how much nonlinearity is present. We see that in glass beads, the R_n values are larger in fully humid samples than in drier samples, while in sand, all the curves seem to overlap, that is, the nonlinearity level seems rather independent of RH. For both sample types, the R_0 and R_1 values fit roughly linearly ($\nu_0 \approx 1$, $\nu_1 \approx 1$) with dynamic stress amplitude. Such scalings for R_0 and R_1 suggest that the y-intercepts on these plots correspond to the hysteretic and quadratic nonlinear parameters α and β, respectively. As for the R_2 values, they scale roughly quadratically ($\nu_2 \approx 2$), which suggest that the y-intercept correspond to the cubic nonlinear parameter δ. Note that for sand, R_2 is rather stress-independent at low stress and starts to increase quadratically only above ~0.1-0.2 MPa (as indicated by the small vertical arrow in Fig. 2f). Based on these scalings, we overlay parallel lines to indicate the value of each nonlinear parameter for a given y-intercept. The three nonlinear parameters α, β and δ dictate the strain-dependence of the elastic modulus M (or equivalently the wave velocity c) according to:

$$\frac{\Delta M}{M_0} = 2\frac{\Delta c}{c_0} = \beta\varepsilon + \delta\varepsilon^2 + \alpha(\varepsilon_0 + \text{sign}(\dot{\varepsilon})\varepsilon)$$

where ε is the dynamic strain, $\dot{\varepsilon}$ is the strain rate, and ε_0 is the dynamic strain amplitude. Because our controlling variable is stress rather than strain, we convert from strain to stress assuming that the nonlinearity is small, i.e., $\sigma = M_0\varepsilon$, where $M_0 = 1$ GPa which corresponds to an average linear elastic modulus for all samples. This allows us to compare the nonlinear parameters with values found in the existing literature where, most of the time, the controlling variable is strain (Guyer & Johnson, 2009).

Harmonic amplitude plots, sorted per samples rather than R_n values, are also included in the supplementary materials (Figs. S6-7). For both sample types, at a given dynamic stress amplitude, we find that R_1 is larger than R_0 and R_2, which is consistent with our previous observation that the slope dominates the nonlinear signatures compared to the offset and the curvature.

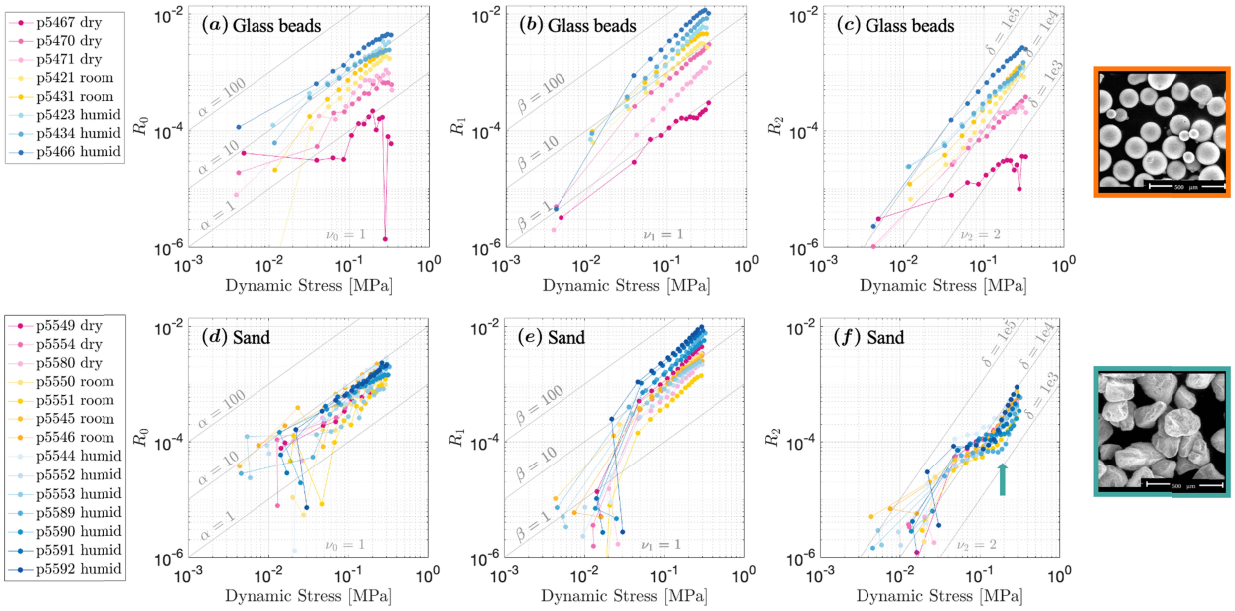

Figure 2. Harmonic amplitudes R_n as a function of dynamic stress amplitude for all glass beads (top row) and sand (bottom row) samples. Only results from the third DAET test are shown for clarity. (a-d) Parameter R_0. The overall scaling is linear [$\nu_0 \approx 1$ in Eq. (2)]. (b-e) Parameter R_1. The overall scaling is roughly linear [$\nu_1 \approx 1$ in Eq. (2)]. (c-f) Parameter R_2. The scaling is roughly quadratic [$\nu_2 \approx 2$ in Eq. (2)]. Note the kink in the curves at ~0.2 MPa for the sand samples – panel f – as pointed out by the small vertical arrow (also see Fig. 4).

We plot the extracted nonlinear parameters α, β, and δ for glass beads and sand samples as a function of RH level in Fig. 3. We find that overall, both materials have a similar range of elastic nonlinearity. However, while all nonlinear parameters increase with RH for glass beads, little variation can be seen in sand. For sand, α and δ exhibit no variation with RH, and only a small increase in β for fully humid samples, on average, although scatter is quite large. We do not know if this increase in β at 100% is real or due to the large scatter; we conducted more experiments at 100% RH than at drier conditions, so the scatter might appear larger for that reason. We are currently designing a new setup where a single sample kept under static load can be monitored while being humidified/dried. By doing so, we anticipate reducing uncertainties by monitoring the elastic nonlinearity of a single sample instead of different samples.

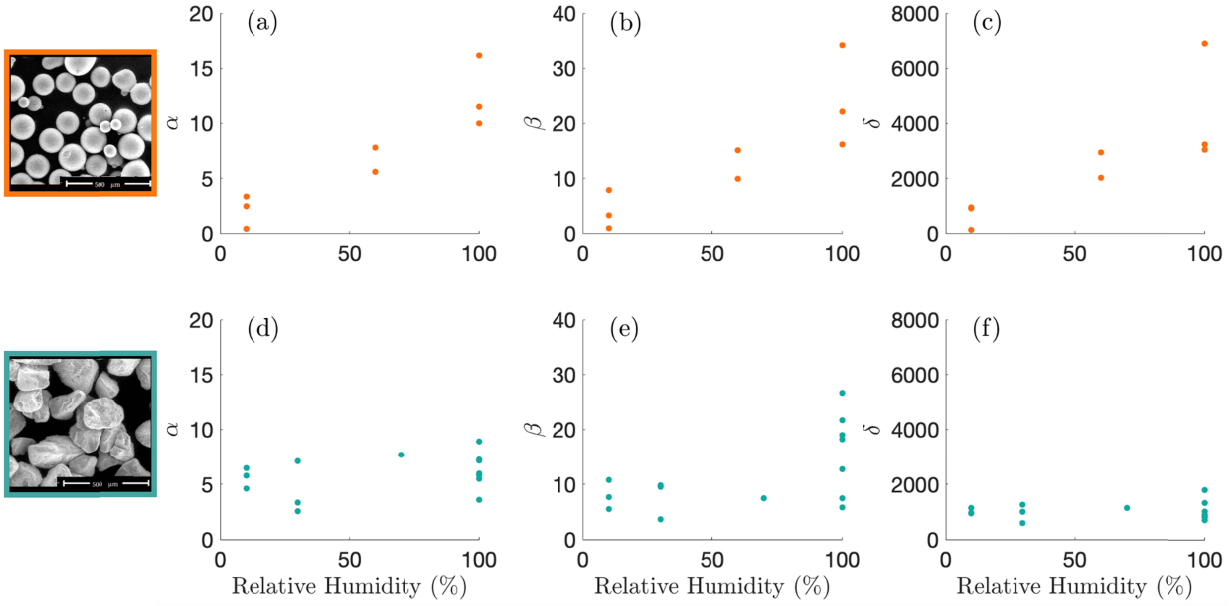

Figure 3. Nonlinear parameters as a function of RH for glass beads (top row) and sand (bottom row). These parameters are related to a_n in Eq. (2), that is, (a)(d) α related to a_0, (b)(e) β related to a_1, and (c)(f) δ related to a_2. Each point represents one DAET test (four tests per experiment). While all nonlinear parameters increase with RH for glass beads, they seem rather independent of RH in sand.

As discussed in the introduction, previous studies (Renaud et al., 2012; Rivière et al., 2015, 2016) suggest that there exists two main physical mechanisms behind the nonlinear elastic properties of granular/damaged solids: the parameter β, (related to R_1) that is likely related to the opening/closing of mesoscopic features such as cracks and grain-grain junctions, while all other parameters (α, related to R_0; δ, related to R_2 as well as hysteresis area (Rivière et al., 2015) might be related to shearing/sliding/partial slip of these same features. In this work, we find that the nonlinear parameters are rather independent of RH in sand, while showing a large dependence of RH in glass beads. This is in line with the interpretation made in our previous study (Gao et al., 2022), hypothesizing that adsorbed water on glass beads pushes the beads apart (similar to a small increase in pore pressure (Gor & Gurevich, 2018; Gor & Neimark, 2010),

making the junctions weaker and more nonlinear. The fact that the elastic nonlinearity does not significantly change with RH in sand might come from grain interlocking, that is, the angular grains prevent adsorbed water from weakening/dilating the sample. Previous results in porous sandstones have shown that adsorbed water on the grains causes tensile deformation and reduced elastic moduli (Amberg & McIntosh, 1952; Guyer & Kim, 2015; Yurikov et al., 2018), although the grains are angular. This is in contradiction with our results in unconsolidated sand, where changes in RH have little effect, but seems to suggest that in sandstones, the changes in RH affect the soft bonds between the grains, rather the bare contacts between grains.

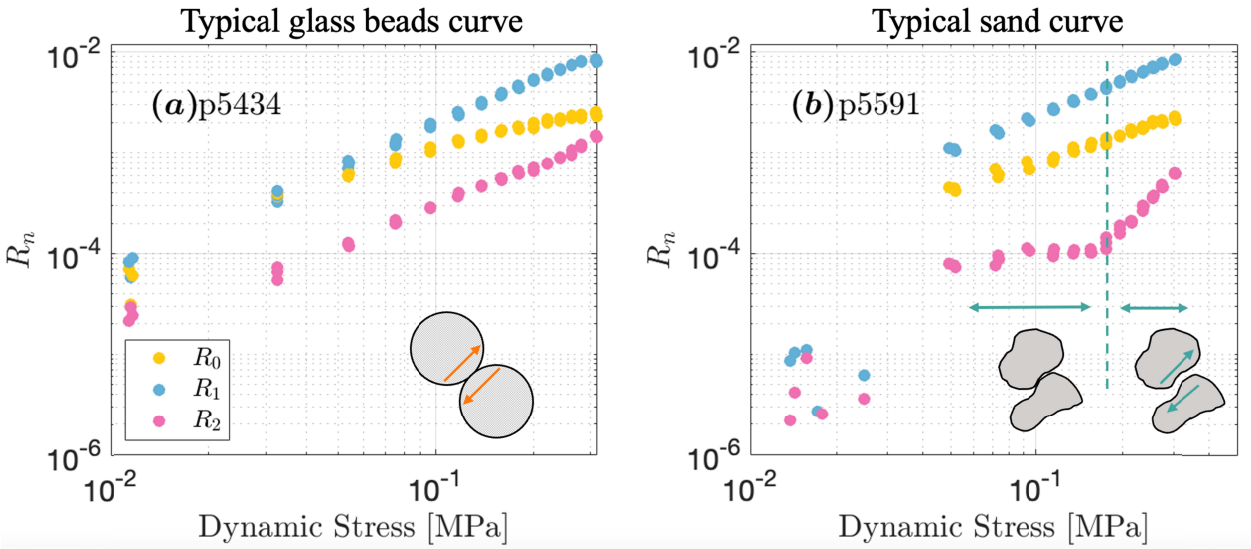

Figure 4. Harmonic amplitudes extracted from the nonlinear signatures on a log-log scale. The parameter R_0 represents the transient elastic weakening, while R_1 and R_2 represent the slope and curvature of the nonlinear signatures. Only the data from DAET oscillation set No. 2, 3, and 4 are shown due to the possible large compaction during the first DAET oscillation set. (a) A typical glass bead sample at 100% RH (b) A typical sand sample at 100% RH.

Finally, we emphasize our previous observation that in sand samples, the parameter R_2 is stress-independent at low dynamic stress amplitudes and starts to increase quadratically for amplitudes larger than ~0.1–0.2 MPa (small arrow in Fig. 3f). In Fig. 4, we show the R_n values vs dynamic stress amplitude for one typical glass bead sample (Fig. 4a) and one typical sand sample (Fig. 4b). We see a clear kink in the curve for R_2 in sand, while it increases monotonically with stress amplitude in glass beads. If R_2, related to the curvature of the nonlinear signatures and the parameter δ, originates from shearing/partial slip of the grain junctions – as we argue – then this suggests that shearing/partial slip is mostly absent at low stress/strain amplitudes due to grain locking, and starts taking place only above a particular stress amplitude (~0.1–0.2 MPa here). In comparison, shearing/partial slip in spherical glass beads likely initiates at much lower dynamic stress/strain amplitudes. Another interesting observation is that other R_n values in sand do not exhibit any such amplitude threshold. Because previous work suggests that β/R_1 is related to one mechanism while all other parameters are related to a second mechanism, we could have

expected both R_0 and R_2 to exhibit an amplitude threshold. This is the not the case and further work would be needed to investigate this discrepancy.

5 Conclusions

In this study, we investigate the effect of grain shape and relative humidity on the nonlinear elastic properties of granular media by conducting experiments on spherical glass beads and angular quartz sand. We found that, compared to glass beads, the elastic nonlinearity of angular sand does not increase significantly with RH, but is rather independent of RH, which we attribute to grain interlocking that prevents adsorbed water from weakening the grain junctions. Furthermore, for one of the nonlinear parameters (δ/R_2) which has been attributed to sliding/partial slip of grain junctions, we observe a sharp amplitude threshold in sand but not in glass beads. This seems to confirm that this nonlinear parameter (δ/R_2) is indeed related to sliding/partial slip of the grain junctions. Below the amplitude threshold, i.e., at low dynamic stress oscillations, the angular grains of sand are locked, and no sliding/partial slip can occur. This mechanism seems to get activated only at larger stress oscillations when the grain junctions unlock.

Acknowledgments

The authors would like to thank Chris Marone for his help with the loading apparatus and many helpful discussions, Steve Swavely for technical support, and David C. Bolton, Srisharan Shreedharan, Clay Wood, Samson Marty, and Raphael Affinito for their help with operating the loading apparatus. This work was partially supported by a grant from the U.S. Department of Energy, Office of Basic Energy Sciences (Award Number DE-SC0017585) to PS, and a grant from the U.S. Department of Energy, Office of Basic Energy Sciences (Award Number DE-SC0022842) to JR.

Open Research

The data and code used in the study are available at Penn State University's Scholar Sphere via [doi:10.26207/ppqc-7d70, https://scholarsphere.psu.edu/resources/0d041b4d-57c9-457c-9525-a7282c63e5f8] with all rights reserved.

References

Abeele, K. V. D., & De Visscher, J. (2000). Damage assessment in reinforced concrete using spectral and temporal nonlinear vibration techniques. *Cement and Concrete Research*, *30*(9), 1453–1464. https://doi.org/10.1016/S0008-8846(00)00329-X

Abeele, K. V. D., Carmeliet, J., Johnson, P. A., & Zinszner, B. (2002). Influence of water saturation on the nonlinear elastic mesoscopic response in Earth materials and the implications to the mechanism of nonlinearity. *Journal of Geophysical Research: Solid Earth*, *107*(B6), ECV 4-1-ECV 4-11. https://doi.org/10.1029/2001JB000368

Amberg, C. H., & McIntosh, R. (1952). A study of adsorption hysteresis by means of length changes of a rod of porous glass. *Canadian Journal of Chemistry*, *30*(12), 1012–1032. https://doi.org/10.1139/v52-121

Astorga, A., Guéguen, P., & Kashima, T. (2018). Nonlinear Elasticity Observed in Buildings during a Long Sequence of Earthquakes. *Bulletin of the Seismological Society of America*, *108*(3A), 1185–1198. https://doi.org/10.1785/0120170289

Bittner, J. A., & Popovics, J. S. (2022). Transient nonlinear vibration characterization of building materials in sequential impact scale experiments. *Frontiers in Built Environment*, *8*, 949484. https://doi.org/10.3389/fbuil.2022.949484

Breazeale, M. A., & Ford, J. (1965). Ultrasonic Studies of the Nonlinear Behavior of Solids. *Journal of Applied Physics*, *36*(11), 3486–3490. https://doi.org/10.1063/1.1703023

Brunet, T., Jia, X., & Johnson, P. A. (2008). Transitional nonlinear elastic behaviour in dense granular media. *Geophysical Research Letters*, *35*(19). https://doi.org/10.1029/2008GL035264

290 Buck, O., Morris, W. L., & Richardson, J. M. (1978). Acoustic harmonic generation at unbonded
291 interfaces and fatigue cracks. *Applied Physics Letters*, *33*(5), 371–373.
292 https://doi.org/10.1063/1.90399
293 Delorey, A. A., Guyer, R. A., Bokelmann, G. H. R., & Johnson, P. A. (2021). Probing the
294 Damage Zone at Parkfield. *Geophysical Research Letters*, *48*(13), e2021GL093518.
295 https://doi.org/10.1029/2021GL093518
296 Feng, X., Fehler, M., Brown, S., Szabo, T. L., & Burns, D. (2018). Short-Period Nonlinear
297 Viscoelastic Memory of Rocks Revealed by Copropagating Longitudinal Acoustic
298 Waves. *Journal of Geophysical Research: Solid Earth*, *123*(5), 3993–4006.
299 https://doi.org/10.1029/2017JB015012
300 Feng, X., Fehler, M., Burns, D., Brown, S., & Szabo, T. L. (2022). Effects of humidity and
301 temperature on the non-linear elasticity of rocks. *Geophysical Journal International*,
302 *231*(3), 1823–1832. https://doi.org/10.1093/gji/ggac292
303 Gao, L., Shokouhi, P., & Rivière, J. (2022). Effect of relative humidity on the nonlinear elastic
304 response of granular media. *Journal of Applied Physics*, *131*(5), 055101.
305 https://doi.org/10.1063/5.0073967
306 Gor, G. Y., & Gurevich, B. (2018). Gassmann Theory Applies to Nanoporous Media.
307 *Geophysical Research Letters*, *45*(1), 146–155. https://doi.org/10.1002/2017GL075321
308 Gor, G. Y., & Neimark, A. V. (2010). Adsorption-Induced Deformation of Mesoporous Solids.
309 *Langmuir*, *26*(16), 13021–13027. https://doi.org/10.1021/la1019247
310 Guyer, R. A., & Johnson, P. A. (1999). Nonlinear Mesoscopic Elasticity: Evidence for a New
311 Class of Materials. *Physics Today*, *52*(4), 30–36. https://doi.org/10.1063/1.882648

312 Guyer, R. A., & Johnson, P. A. (2009). *Nonlinear Mesoscopic Elasticity*. Weinheim, Germany:
313 Wiley-VCH Verlag GmbH & Co. KGaA. https://doi.org/10.1002/9783527628261
314 Guyer, R. A., & Kim, H. A. (2015). Theoretical model for fluid-solid coupling in porous
315 materials. *Physical Review E*, *91*(4), 042406.
316 https://doi.org/10.1103/PhysRevE.91.042406
317 Hillers, G., Retailleau, L., Campillo, M., Inbal, A., Ampuero, J.-P., & Nishimura, T. (2015). In
318 situ observations of velocity changes in response to tidal deformation from analysis of the
319 high-frequency ambient wavefield. *Journal of Geophysical Research: Solid Earth*,
320 *120*(1), 210–225. https://doi.org/10.1002/2014JB011318
321 Jia, X., Brunet, Th., & Laurent, J. (2011). Elastic weakening of a dense granular pack by acoustic
322 fluidization: Slipping, compaction, and aging. *Physical Review E*, *84*(2), 020301.
323 https://doi.org/10.1103/PhysRevE.84.020301
324 Jin, J., Johnson, P. A., & Shokouhi, P. (2020). An integrated analytical and experimental study of
325 contact acoustic nonlinearity at rough interfaces of fatigue cracks. *Journal of the*
326 *Mechanics and Physics of Solids*, *135*, 103769.
327 https://doi.org/10.1016/j.jmps.2019.103769
328 Johnson, P., & Sutin, A. (2005). Slow dynamics and anomalous nonlinear fast dynamics in
329 diverse solids. *The Journal of the Acoustical Society of America*, *117*(1), 124–130.
330 https://doi.org/10.1121/1.1823351
331 Johnson, P. A., & Jia, X. (2005). Nonlinear dynamics, granular media and dynamic earthquake
332 triggering. *Nature*, *437*(7060), 871–874. https://doi.org/10.1038/nature04015

Kim, G., Kim, J.-Y., Kurtis, K. E., & Jacobs, L. J. (2017). Drying shrinkage in concrete assessed by nonlinear ultrasound. *Cement and Concrete Research*, *92*, 16–20. https://doi.org/10.1016/j.cemconres.2016.11.010

Kim, J.-Y., Jacobs, L. J., Qu, J., & Littles, J. W. (2006). Experimental characterization of fatigue damage in a nickel-base superalloy using nonlinear ultrasonic waves. *The Journal of the Acoustical Society of America*, *120*(3), 1266–1273. https://doi.org/10.1121/1.2221557

Lacouture, J.-C., Johnson, P. A., & Cohen-Tenoudji, F. (2003). Study of critical behavior in concrete during curing by application of dynamic linear and nonlinear means. *The Journal of the Acoustical Society of America*, *113*(3), 1325–1332. https://doi.org/10.1121/1.1543927

Langlois, V., & Jia, X. (2014). Acoustic probing of elastic behavior and damage in weakly cemented granular media. *Physical Review E*, *89*(2), 023206. https://doi.org/10.1103/PhysRevE.89.023206

Manogharan, P., Wood, C., Marone, C., Elsworth, D., Rivière, J., & Shokouhi, P. (2021). Nonlinear elastodynamic behavior of intact and fractured rock under in-situ stress and saturation conditions. *Journal of the Mechanics and Physics of Solids*, *153*, 104491. https://doi.org/10.1016/j.jmps.2021.104491

Matlack, K. H., Kim, J.-Y., Jacobs, L. J., & Qu, J. (2015). Review of Second Harmonic Generation Measurement Techniques for Material State Determination in Metals. *Journal of Nondestructive Evaluation*, *34*(1), 273. https://doi.org/10.1007/s10921-014-0273-5

McCall, K. R., & Guyer, R. A. (1994). Equation of state and wave propagation in hysteretic nonlinear elastic materials. *Journal of Geophysical Research: Solid Earth*, *99*(B12), 23887–23897. https://doi.org/10.1029/94JB01941

356 Ostrovsky, L. A., & Johnson, P. A. (2001). Dynamic nonlinear elasticity in geomaterials. *La*
357 *Rivista Del Nuovo Cimento*, *24*(7), 1–46. https://doi.org/10.1007/BF03548898
358 Payan, C., Ulrich, T. J., Le Bas, P. Y., Saleh, T., & Guimaraes, M. (2014). Quantitative linear
359 and nonlinear resonance inspection techniques and analysis for material characterization:
360 Application to concrete thermal damage. *The Journal of the Acoustical Society of*
361 *America*, *136*(2), 537–546. https://doi.org/10.1121/1.4887451
362 Renaud, G., Callé, S., & Defontaine, M. (2009). Remote dynamic acoustoelastic testing: Elastic
363 and dissipative acoustic nonlinearities measured under hydrostatic tension and
364 compression. *Applied Physics Letters*, *94*(1), 011905. https://doi.org/10.1063/1.3064137
365 Renaud, G., Le Bas, P., Ten Cate, J. A., Ulrich, T. J., Carey, J. W., Han, J., et al. (2011).
366 Dynamic Measures of Elastic Nonlinear (Anelastic) Behavior: Dynamic Acousto-
367 Elasticity Testing (DAET). *AGU Fall Meeting Abstracts*, *51*, MR51A-2151.
368 Renaud, G., Le Bas, P.-Y., & Johnson, P. A. (2012). Revealing Highly Complex Elastic
369 Nonlinear (anelastic) Behavior of Earth Materials Applying a New Probe: Dynamic
370 Acoustoelastic Testing: A New Probe for Elasticity in Rocks. *Journal of Geophysical*
371 *Research: Solid Earth*, *117*(B6). https://doi.org/10.1029/2011JB009127
372 Renaud, G., Rivière, J., Haupert, S., & Laugier, P. (2013). Anisotropy of dynamic
373 acoustoelasticity in limestone, influence of conditioning, and comparison with nonlinear
374 resonance spectroscopy. *The Journal of the Acoustical Society of America*, *133*(6), 3706–
375 3718. https://doi.org/10.1121/1.4802909
376 Rivière, J., Shokouhi, P., Guyer, R. A., & Johnson, P. A. (2015). A set of measures for the
377 systematic classification of the nonlinear elastic behavior of disparate rocks. *Journal of*

Geophysical Research: Solid Earth, *120*(3), 1587–1604. https://doi.org/10.1002/2014JB011718

Rivière, J., Pimienta, L., Scuderi, M., Candela, T., Shokouhi, P., Fortin, J., et al. (2016). Frequency, pressure, and strain dependence of nonlinear elasticity in Berea Sandstone. *Geophysical Research Letters*, *43*(7), 3226–3236. https://doi.org/10.1002/2016GL068061

Shokouhi, P., Rivière, J., Lake, C. R., Le Bas, P.-Y., & Ulrich, T. J. (2017). Dynamic acousto-elastic testing of concrete with a coda-wave probe: comparison with standard linear and nonlinear ultrasonic techniques. *Ultrasonics*, *81*, 59–65. https://doi.org/10.1016/j.ultras.2017.05.010

Shokouhi, P., Jin, J., Wood, C., Rivière, J., Madara, B., Elsworth, D., & Marone, C. (2020). Dynamic Stressing of Naturally Fractured Rocks: On the Relation Between Transient Changes in Permeability and Elastic Wave Velocity. *Geophysical Research Letters*, *47*(1), e2019GL083557. https://doi.org/10.1029/2019GL083557

Tadavani, S. K., Poduska, K. M., & Malcolm, A. E. (2020). A non-linear elastic approach to study the effect of ambient humidity on sandstone. *Journal of Applied Physics*, *128*(24), 244902. https://doi.org/10.1063/5.0025936

TenCate, J. A., Abeele, K. V. D., Shankland, T. J., & Johnson, P. A. (1996). Laboratory study of linear and nonlinear elastic pulse propagation in sandstone. *The Journal of the Acoustical Society of America*, *100*(3), 1383–1391. https://doi.org/10.1121/1.415985

TenCate, J. A., Malcolm, A. E., Feng, X., & Fehler, M. C. (2016). The effect of crack orientation on the nonlinear interaction of a *P* wave with an *S* wave. *Geophysical Research Letters*, *43*(12), 6146–6152. https://doi.org/10.1002/2016GL069219

Williams, C., Borigo, C., Rivière, J., Lissenden, C. J., & Shokouhi, P. (2022). Nondestructive Evaluation of Fracture Toughness in 4130 Steel Using Nonlinear Ultrasonic Testing. *Journal of Nondestructive Evaluation*, *41*(1), 13. https://doi.org/10.1007/s10921-022-00846-5

Yurikov, A., Lebedev, M., Gor, G. Y., & Gurevich, B. (2018). Sorption-Induced Deformation and Elastic Weakening of Bentheim Sandstone. *Journal of Geophysical Research: Solid Earth*, *123*(10), 8589–8601. https://doi.org/10.1029/2018JB016003